


Numerical analysis of the hydrodynamic characteristics of the accelerating and decelerating ducted propeller

Amir Hossein Razaghian¹, Hassan Ghassemi² 

¹ Sharif University of Technology, Department of Mechanical Engineering, Tehran, Iran

² Amirkabir University of Technology, Department of Maritime Engineering, Tehran, Iran

 corresponding author's email: gasemi@aut.ac.ir

Key words: accelerating and decelerating ducted propeller, pressure coefficient, hydrodynamics characteristics

Abstract

This paper investigates the open-water characteristics of the 5-blade propeller with accelerating and decelerating ducts using the Reynolds-Averaged Navier-Stokes (RANS) equation code. In the first step, numerical open-water hydrodynamic characteristics of the propeller in the absence of a duct were validated using the available experimental data. The shear stress transport (SST) turbulence model was chosen, which shows less error in thrust and torque coefficients than others. In the second step, two accelerating and decelerating ducts, namely ducts 19A and N32, were modeled. In these simulations, the clearance value was selected at 3 percent of the propeller's diameter and uniform-flow conditions were assumed.

After analysis of the mesh sensitivity for the propeller thrust, the results were compared to the corresponding open-water condition values. In this regard, results of the hydrodynamic coefficients, pressure distribution, and coefficients on the propeller-blade surface and ducts were also analyzed and discussed.

Introduction

Since 1930, ducted propellers have been used on tugs, push-boats, trawlers, and torpedoes since. They have also been used in large vessels like tankers and bulk carriers in order to improve the hydrodynamic characteristics in heavy conditions. In an accelerating duct, the flow velocity is increased due to characteristics of the duct and the amount of duct drag force is lower than the lift force, especially in heavy conditions.

The use of an accelerating type of duct, in combination with the propeller, can lead to lower propeller damage and is a better way of increasing propulsive efficiency by axial-losses reduction in a bollard condition. Decelerating ducts decrease the propulsive efficiency but they postpone cavitation inception and the risk of vibration decreases. Therefore, the appropriate condition for military purposes in marine structures is provided. For accelerating

ducts, in general, the ratio of thrust generated by the duct to that of the total propulsor varies by advance coefficients. Also, it may decrease with respect to the open-flow propeller thrust in the same condition for a higher advanced coefficient. Moreover, the propulsor torque generated by the propeller remains constant in both circumstances and is provided only by the propeller. Figure 1 shows the generated lift, thrust, and circulation around decelerating and accelerating ducts.

The history of ducted-propeller analysis goes back to experimental results performed by Stipa (Stipa, 1931) and by Kort (Kort, 1934). In fact, these researchers showed the efficiency increases in accelerating-ducted propellers for heavy conditions. Later, Sparenberg (Sparenberg, 1969) demonstrated that the presence of a duct of finite length around the actuator disc, regardless of its type, in axisymmetric flow has an influence of the second order by accelerating and decelerating the flow, depending on duct

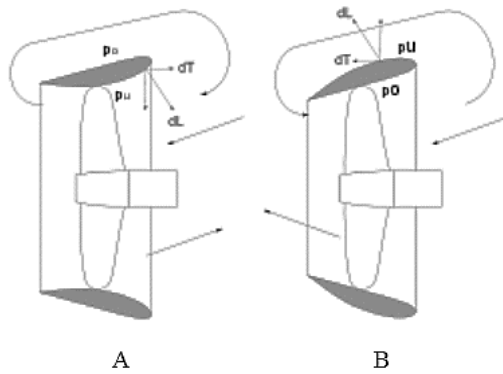


Figure 1. An acceleration duct (A) and a deceleration duct (B)

section profiles. Furthermore, it was also shown that these effects mainly depend on advanced-coefficient ratio and advance velocity, while in the case of light loading, the main efficiency comes from the disk.

In recent years, RANS equations have been widely used by several research groups. For instance, Sanchez-Caja et al. (Sanchez-Caja, Rautahaimo & Siikonen, 2000) used a RANS equation solver to simulate incompressible viscous flow around a propeller in the presence of a duct. In addition, Abdel-Maksoud & Heinke (Abdel-Maksoud & Heinke, 2003) have also investigated scale effects on ducted propellers numerically. Krasilnikov et al. (Krasilnikov et al., 2007), as another example, developed new mesh-generation techniques to study scale effects on the ducted propellers by a commercial RANS equation solver in the numerical analysis. On the other hand, recently, Arazgaldi et al. (Arazgaldi, Hajilouy & Farhanieh, 2009) presented a numerical investigation of solving the RANS equation and used a cavitation model to determine characteristics of two non-cavitating, four- and three-bladed propellers. In this study, the cavitation breakdown was calculated using the CFD method and the obtained numerical results were compared with the experimental ones adopted by the K23 cavitation tunnel at the Sharif University of Technology. The comparison study showed a fairly good agreement. Moreover, Salvatore et al. (Salvatore, Greco & Calcagni, 2011) developed a BEM code entitled INSEAN-PFC to determine inviscid flows in an arbitrary motion for a fluid at rest. The propeller's wake-velocity field was captured and cavitation in uniform flow was predicted. Furthermore, Celik et al. (Celik, Dogrul & Arıkan, 2011) obtained the optimum accelerating (19A) and decelerating (N32) conventional duct geometry of the four-blade propeller propulsion efficiency using the lifting-surface theory method. Many turbulence models have been studied recently to determine the

best setting of numerical results based on the CFD method. In this regard, Subhas et al. (Subhas et al., 2012) used a standard $K - \epsilon$ turbulence model in the CFD code Fluent 6.3 commercial software to set the hydrodynamic characteristics of a INSEAN E779a model propeller in both cavitating and non-cavitating conditions. In the numerical analysis of propellers, by comparing the BEM method and CFD method, Gaggero et al. (Gaggero et al., 2013) applied the coupled lifting line/panel method and hybrid design approach for the design of decelerating-ducted propellers to study the cavitation characteristics of propellers, comparing with experimental results. Finally, it was suggested that the RANS equation solver performed better in the same condition and that the panel method was only capable of capturing vortex presence. Moreover Muszyński & Strzelczyk (Muszyński & Strzelczyk, 2013) investigated different duct models in combination with the propeller, in order to specify hydrodynamic characteristics of the propeller. In this research, results of some selected geometries are published and a distribution of velocity for one specific, ducted propeller compared with numerical results, based on the finite volume method. Furthermore, the CFD method was used by Baltazar et al. (Baltazar et al., 2013) to compare the numerical open-water characteristics of ducted propellers with panel method results. The equations were discretized using the finite-volume method and finally the panel-method results were in good agreement with CFD-analysis results in the same condition. Koh et al. (Koh et al., 2015) designed a duct section profile for better characteristics of fishing-boat propellers at a highly-advanced coefficient that is more efficient than 19A. Their experimental results showed a maximum 23% increase in the propeller thrust at highly-advanced ratios, unlike the 19A ducted propeller. Neural networks are one of the newest methods to analyze propeller open-water characteristics. In this regard, Valcic & Dejhala (Valcic & Dejhala, 2015) published the open-water characteristics of four-blade Ka-series located in the 19A duct, using this method. In order to design this solver system, a two-layered, feed-forward, neural-network system was trained. Finally, the data of the azimuth thruster was published. In order to determine propeller pressure distribution, He et al. (He et al., 2015) analyzed the hydrodynamic characteristic of the ducted propeller with MBHM & RSM methods. These numerical results were compared with the standard $K - \epsilon$ two-equation model for the two JD7704+Ka4-55 propellers. Finally, it was shown that MBHM & RSM methods are more usable for determination

of ducted-propeller, hydrodynamic characteristics. Moreover, Majdfar, Ghassemi & Forouzan (Majdfar, Ghassemi & Forouzan, 2015) investigated the variations of nozzle 19A duct length and angle on the Kaplan propeller using a RANS equation solver. Also, Majdfar & Ghassemi (Majdfar & Ghassemi, 2016) extended the calculations of the hydrodynamic characteristics of a ducted propeller operating in oblique flow that is under publication.

In the present work, the RANS equation solver is employed to calculate the hydrodynamic characteristics for the B-series, 5-blade propeller with accelerating (19A) and decelerating (N32) ducts. The investigation is based on the SST turbulence model. A review of the computational equations and methodology is presented and the accuracy of the results is discussed. The simulation results of pressure distribution, velocity field, and open-water characteristics are compared for the two different ducts.

Numerical methods and governing equations

In this paper, the conservation form of unsteady Navier-Stokes equations along with momentum equations has been numerically solved to obtain the velocity and pressure fields in global and local forms.

In this regard, first, the conservation of mass principle has been considered, which leads to the following differential equation in terms of the velocity field and the mass density, and is known as the continuity equation:

$$\frac{\partial \rho}{\partial t} + \frac{\partial}{\partial x_i} (\rho u_i) = 0 \quad (1)$$

where ρ is the density of the fluid while u_i shows the fluid velocity-vector components. Furthermore, the principal of the conservation of linear momentum was also satisfied by solving the following well-known global Navier-Stokes equation:

$$\frac{\partial}{\partial t} (\rho u_i) + \frac{\partial}{\partial x_j} (\rho u_j u_i) = -\frac{\partial p}{\partial x_i} + \frac{\partial \tau_{ij}}{\partial x_j} + \rho g_i \quad (2)$$

where p denotes pressure and g is the gravitational acceleration. In fact, as equations (1) and (2) are coupled, these equations should be solved simultaneously and in an iterative manner. The obtained results, then, have been employed as inputs of a post-processing analysis in local conditions. It should be noted that in case of incompressible flow, the density is constant and the propeller flow is considered to be steady. The RANS equations are solved by the finite

volume method while the SST turbulence model was utilized to compute the transport of the turbulent shear stresses. The SST model was selected since it has been widely used by different researchers in the past and its proficiency and reliability in predicting the flow separation has been well demonstrated. Moreover, the multiple rotating reference frame (MRF) method is used in time limitation problems and the complex geometry of domain and boundaries for ducted propellers numerical investigations.

It is well accepted that the hydrodynamic propeller operation can be modeled by the following non-dimensional equations:

$$K_{T_D} = \frac{T_D}{\rho n^2 D^4}, K_{T_p} = \frac{T_p}{\rho n^2 D^4}, K_T = \frac{T_D + T_p}{\rho n^2 D^4} \quad (3)$$

$$K_Q = \frac{Q}{\rho n^2 D^5} \quad (4)$$

$$\eta = \frac{K_T J}{K_Q 2\pi}, J = \frac{V_A}{n D} \quad (5)$$

where K_{TD} denotes the duct thrust coefficient, K_{Tp} shows propeller thrust coefficient, K_T is the total thrust coefficient, K_Q represents Propulsive torque coefficient, J is advanced ratio, η is the propulsive efficiency, n denotes propeller revolution, D is propeller diameter, T_D is the duct thrust and T_p shows the propeller thrust. Consequently, it can be possible to compare results for the open propeller and the ducted propellers.

Propeller and duct-geometry modeling

In this paper, the influence of two types of ducts was investigated on propeller characteristics. In order to specify the most suitable modeling method for finite difference calculations, the open-water properties of 5-blade, expanded-area ratio of 0.7 are obtained by different numerical methods have been compared with the available experimental results. This comparison study showed that the SST turbulence model is the best one. The details of these numerical simulations have been given in next Section of this paper. The two ducts have been selected in a way that cover both types of accelerating (19A) and decelerating (N32) ones, which are the most common conventional duct profile sections.

The contribution of 19A duct thrust on total propulsive characteristics and produced drag, as the speed of advance increases, have been widely investigated. The results are available especially for Kaplan-type propellers. However, very little

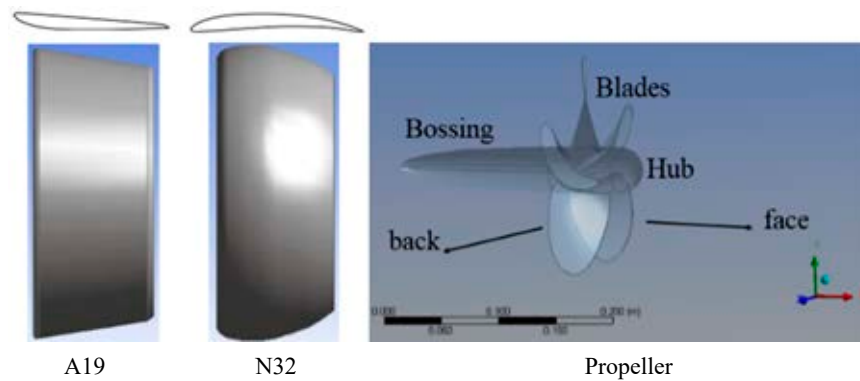


Figure 2. A schematic representation of the propeller and decelerating and accelerating ducts

information is available for propeller characteristics, even in combination with conventional nozzles. Consequently, the results of this research can be of great help in design of the propellers. Moreover, in the current research, the propeller has been investigated and their geometry data are reported in Table 1. The main geometry data of the two ducts are given in Table 2.

Table 1. Main geometry data of the propeller

Parameter	Value
Number of Blades (Z)	5
Expanded Area Ratio (EAR)	0.7
Pitch-Diameter Ratio (P/D)	1.0
Propeller Diameter ($D = 2R$)	0.2 m
Propeller type	B-series

Table 2. Main geometry data of the duct

Parameter	Value
Duct diameter	0.212 m
Duct length	0.106 m
L/D (for duct)	0.5
Clearance between duct and propeller	0.03D
Duct types	19A and N32

Furthermore, Figure 2 depicts the propeller, both ducts (accelerating and decelerating), and the section profiles of the ducts.

Solver settings and validation study

In the present numerical study, the steady-state RANS equations solved for the blades, hub, bossing, ducts, and domains with 3 different finite-volume methods, namely SST, $K - \epsilon$, and $K - \omega$ turbulence models. These models were utilized to minimize the errors between rotating and stationary surfaces. The obtained results showed that the best agreement has been obtained for the open propeller employing the

SST model and hence this model was selected for the characteristics analyses of the ducted propellers. In fact, the SST model is the combinational and robust eddy- viscosity turbulence model to compute the transport of the turbulent shear stresses, using $K - \omega$ in the boundary layer of domains and accomplishing $K - \epsilon$ equations out of layer for shear flow.

The propeller is placed in a cylindrical-flow field containing proper dimensions in the range of the other research's flow-field dimensions. For the propeller, the domain cylinder diameter is $3.5D$, and the vertical axis ($x = 0$) is set to $2.5D$ ahead of inlet plane (upstream) and placed $7.5D$ behind the outlet plane (downstream) shown in Figure 3.



Figure 3. Computational domain

The B-series propellers were designed and tested at the Netherlands Ship Model Basin (NSMB) in Wageningen. The open-water characteristics of 120 propeller models of the B-series were tested at NSMB and analyzed with multiple polynomial regression analysis, Bernitsas et al. (Bernitsas et al., 1981). For the present results validation, B-series propeller (B5-0.7 means $Z = 5$ and EAR = 0.7) selected. A comparison of the open-water characteristics of the B-series propeller with three turbulence models is presented in Figure 4. The results show that thrust and torque coefficients using the SST-turbulence model has less error relative the two other models. The mesh-sensitivity analysis for the SST turbulence model is shown in Figure 5. The propeller thrust is considered as the convergence criteria. Table 3 is given the thrust and y^+ at various mesh numbers that converged by about 9 million meshes.

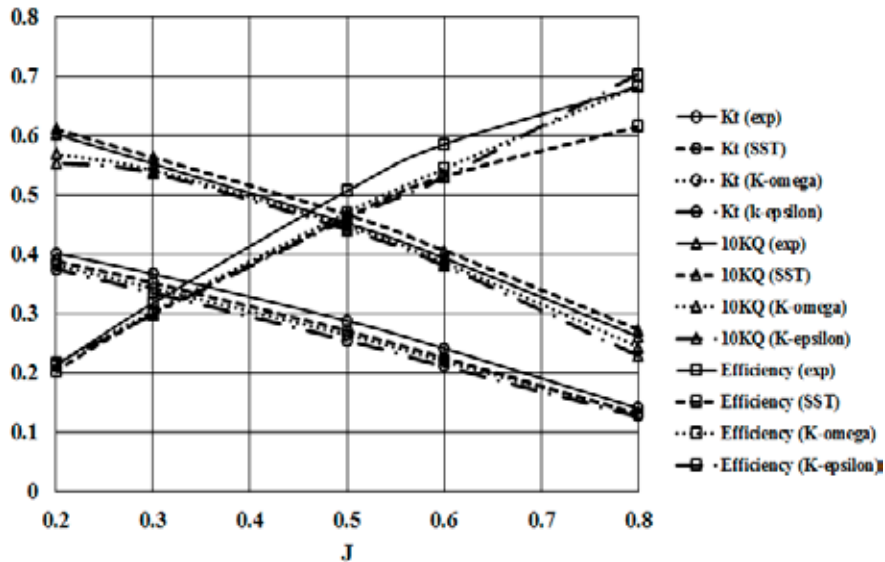


Figure 4. Comparison of the open-water characteristics of the B-series propeller with three turbulence models

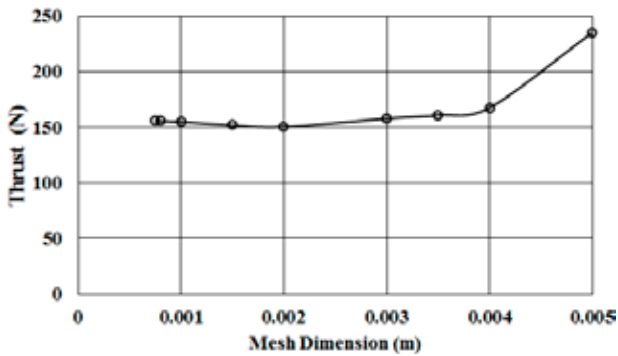


Figure 5. Mesh sensitivity analysis of thrust ($J = 0.3$)

Table 3. Convergence of the thrust by mesh numbers and the value of the y^+

Thrust [N]	y^+	Mesh Numbers
234	2.9	4.3 millions
169	2.4	5.7 millions
162	2.37	6 millions
159	2.26	6.4 millions
150	2	7 millions
156	2.06	7.3 millions
158	2.112	8.7 millions
159	2.111	9 millions
159	2.111	9.1 millions

It should be noted that the reported values of the total mesh numbers in Table 3 have been rounded

to the hundred-thousand. It is important to also note that the mesh dimension for each calculation is the minimum one-side length of the 3D cells that are reported in Figure 5.

It is obvious that the SST turbulence model has higher accuracy compared to the other turbulence models, based on numerical results (Figure 4) for the open-water propeller thrust and torque. The related thrust-coefficients and torque-coefficients errors for different advance ratios are illustrated in Table 4.

In the first step, numerical open-water propeller results without the duct have been validated with experimental results. According to the results, SST has been used that shows a maximum of 7% and 4% errors in thrust coefficient and torque coefficient. This comparison concludes acceptable agreement. According to the published data, an accurate CFD method together with a SST turbulence model is used for the next step of the ducted propeller analysis. The domain geometries for the ducted propeller are similar to the open-water ones.

Ducted propeller results

In this section, the SST turbulence model has been employed in order to compare the characteristics of

Table 4. Comparison of the three turbulence models for open-water parameter errors

J	SST Turbulence model		K-omega Turbulence model		K-epsilon Turbulence model	
	Kt error (%)	KQ error (%)	Kt error (%)	KQ error (%)	Kt error (%)	KQ error (%)
0.8	5.98	4.11	6.51	6.85	9.54	12.33
0.6	6.45	3.05	8.9	2.04	12.46	3.31
0.5	5.78	3.16	8.25	1.18	11.46	2.37
0.3	4.04	1.94	6.5	1.94	8.6	2.91
0.2	3.23	1.4	4.89	5.64	6.62	8.01

the two selected, frequently-used ducts, namely 19A and N32. In this regard, the CFD method, in conjunction with the SST turbulence model, was applied. The finite volume models were discretized by an unstructured mesh in which the cell sizes were small near the blades and ducts (0.8 mm) and increased toward the wall boundary in the cylinder domain, up to 2 cm; it has around nine millions meshes over the entire domains for both 19A and N32 geometries. Figure 6 illustrates the applied mesh pattern for the two models.

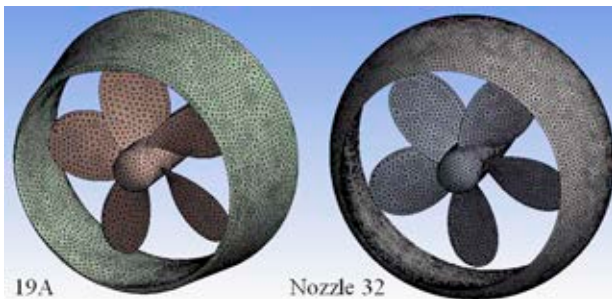


Figure 6. Unstructured mesh cells on ducted propellers

It should also be noted that the dimensionless properties of the numerical studies performed in this section are the same as those given for the open-propeller model in section 4 of this study.

Hydrodynamic characteristics

In this section, the thrust variations with respect to the propeller revolution speed have been explored for the two ducted and open-water 5-blade propeller, assuming a constant velocity of 1 m/s in the inlet plane. The propeller revolution speed was varied between a low RPM of 375 to a high RPM of 1500,

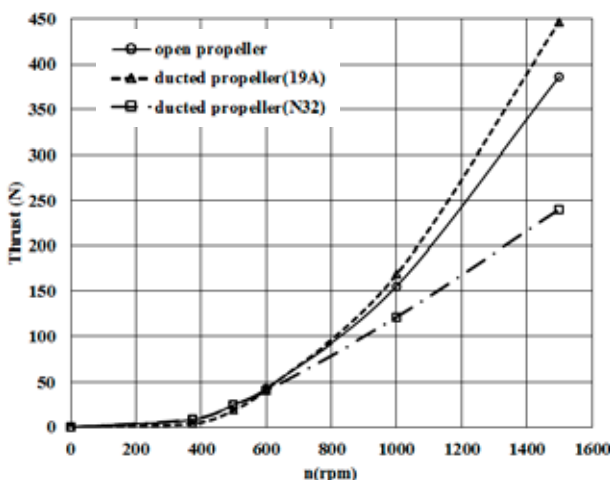


Figure 7. Open-water and ducted propeller thrust comparison

which covers bollard and free-running conditions. There are important differences of total propulsive thrust due to the operation of accelerating and decelerating in different advanced ratios. The total propulsive thrusts for different propellers' revolutions are shown in Figure 7, compared with the open propeller.

Based on Figure 7, it can be seen that the total thrust of the 19A ducted propeller is raised by increasing the rotational speed of the propeller and ascending above the open curve at 600 RPM. In contrast, the total thrust of the N32 ducted propeller started to drop under the open curve at the same condition. It can also be observed that the ducts have no effect of propulsion in this speed of rotation. The effects of the N32 and 19A ducts on the total thrust coefficients are also shown in Figure 8, for the sake of comparison.

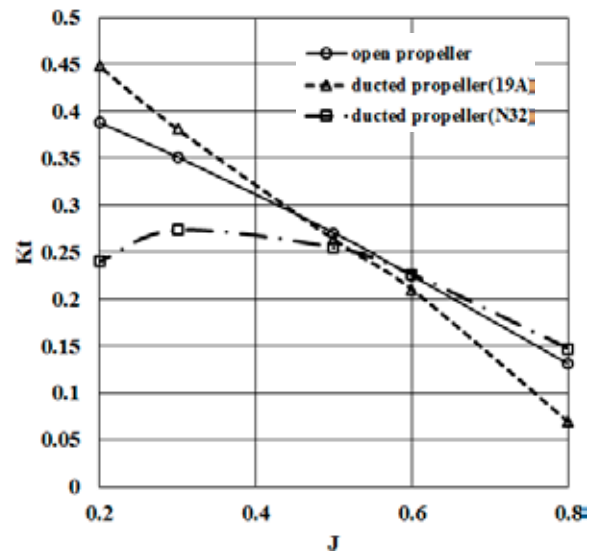


Figure 8. Total thrust coefficient comparison of ducted propellers

According to Figure 8, the 19A ducted propeller can efficiently operate in lower advance ratios (< 0.45) by increasing the total thrust. The 19A force on the flow is in the same direction with the propeller and overcomes nozzle-drag force. Eventually, the summation of the propeller and 19A permanent thrusts was more than the open-propeller thrust near the bollard condition. The highest percentage of the thrust increase is 15.5 percent at $J = 0.2$, extracted from the numerical computations. The N32 ducted propeller, however, operates in the opposite direction of the accelerating 19A duct. Moreover, it can also be observed that the total thrust increase of 12.1 percent occurred in $J = 0.8$, in which the 19A propulsive thrust is about 47 percent less than the open-propeller thrust. Accordingly, by considering open-water

efficiency alone for both ducts, the 19A duct in combination with the 5-blade propeller is appropriate for heavy conditions like trawlers, while the N32 ducted propeller is effective for higher advance ratios like torpedoes.

Distribution of pressure coefficient for the propeller blades and ducts

In this section, the chordwise-pressure-coefficient distribution of the propeller and ducts has been plotted. As the numerical solution, the steady-state accurate computations using the open-water procedure are considered so that the pressure-coefficient distributions are determined in three radial sections

of the propeller blade ($x = 0.3, 0.7, 0.9$). The results have been given for extreme conditions near the bollard one ($J = 0.2$) at the first level and $J = 0.8$ in the next step. Figure 9 illustrates the comparison of pressure-coefficient distribution of the blade at $x = 0.3, 0.7, 0.9$ for the 19A ducted propeller in 0.2 advance ratio; similar graphs for $J = 0.2$ are shown in Figure 10. From Figure 10, it can be seen that for all the x values, a sudden pressure increase happened due to the entrance of the blade's leading edge into the uniform flow and its impact on the uniform flow. As the distance to the root section increases, the peak pressure rises, considering constant speed of advance velocity.

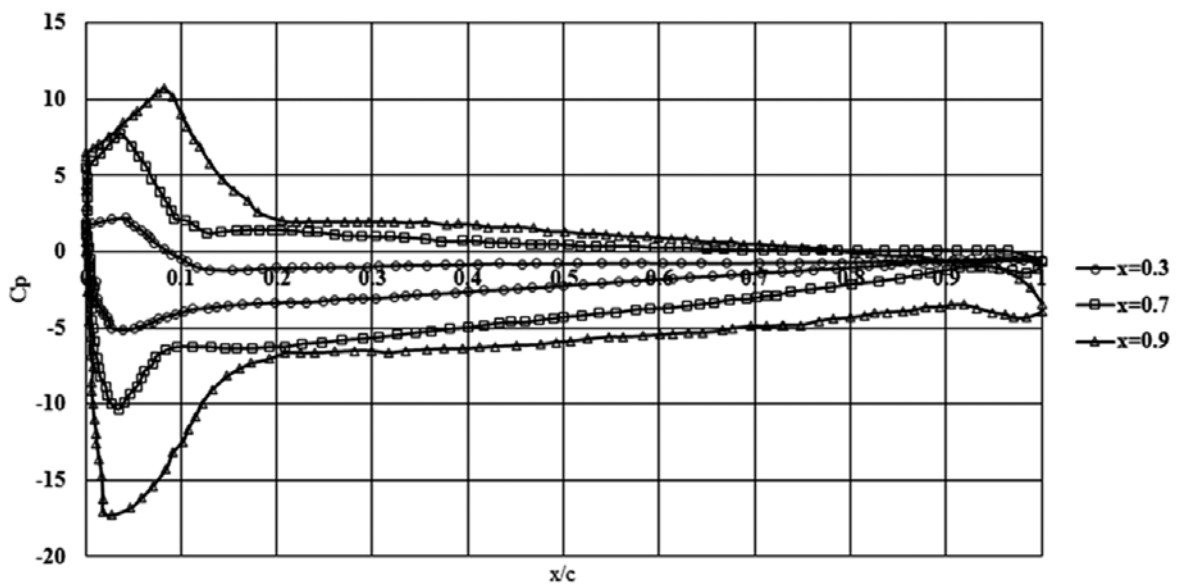


Figure 9. Pressure coefficient comparison of the 19A ducted propeller blade ($J = 0.2$)

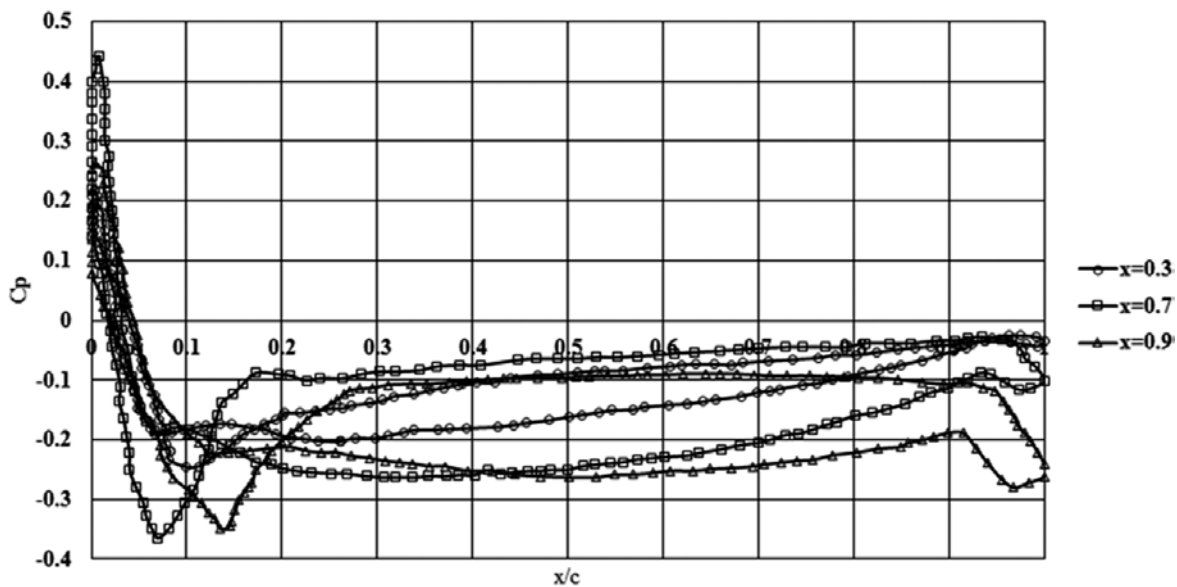


Figure 10. Pressure coefficient comparison of the 19A ducted propeller blade ($J = 0.8$)

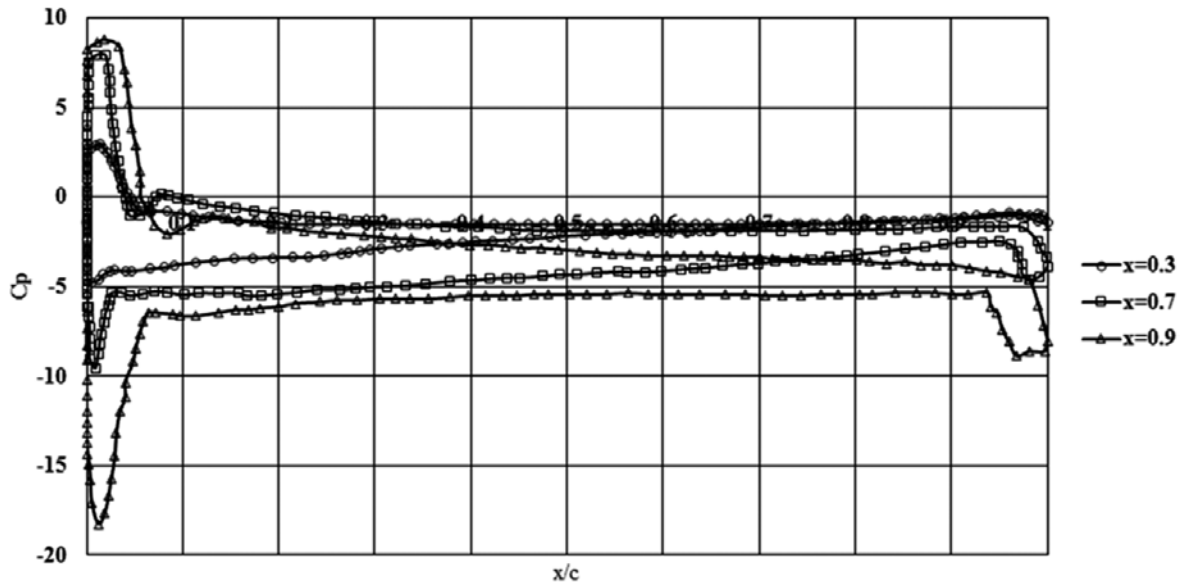


Figure 11. Pressure coefficient comparison of the N32 ducted propeller blade ($J = 0.2$)

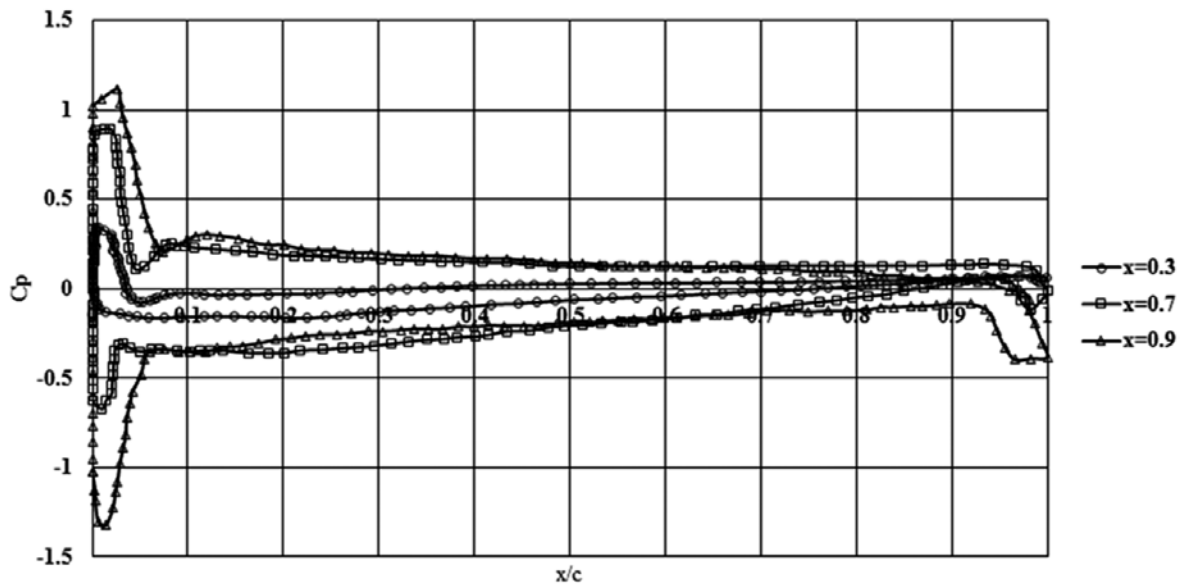


Figure 12. Pressure coefficient comparison of the N32 ducted propeller blade ($J = 0.8$)

Moreover, similar numerical studies have also been performed for the N32 ducted propeller and the obtained results are presented in Figures 11 and 12 for advance ratios of 0.2 and 0.8, respectively.

Concerning the negative-pressure fluctuations in the aforementioned figures and due to a higher propeller-thrust magnitude for the duct 19A than N32 in $J = 0.2$, the total pressure-coefficient distributions of the propeller blade are illustrated in Figure 13.

The similar numerical calculations have been implemented for an advanced ratio of 0.8, shown in Figure 14.

Based on the numerical analyses, the propeller inside the duct N32 produces more thrust than the

duct 19A in $J = 0.8$. This is mainly due to the greater discrepancy between pressure coefficients on pressure and suction sides of the blade in the N32 duct. Figure 15 presents the comparison of pressure-coefficient distributions on the two ducts for $J = 0.2$. From this figure, it can be observed that there is almost a significant difference between the 19A profile-section peak pressure which occurs near the leading edge, unlike the N32.

Pressure contours

Besides the above presented applications, in this subsection, the pressure contour of the ducted

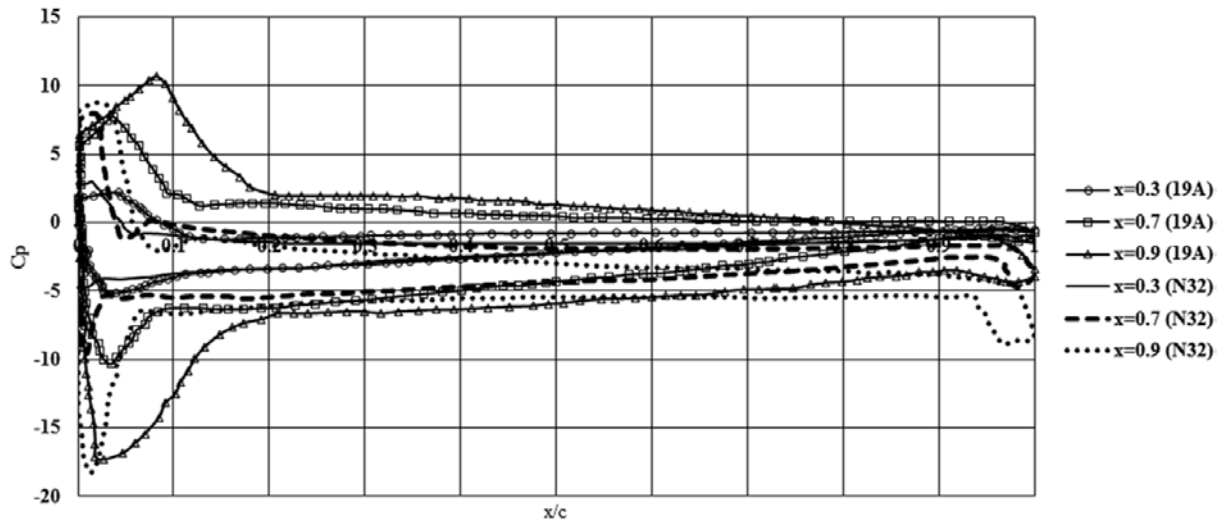


Figure 13. Comparison of the two ducted propeller blade pressure coefficient ($J = 0.2$)

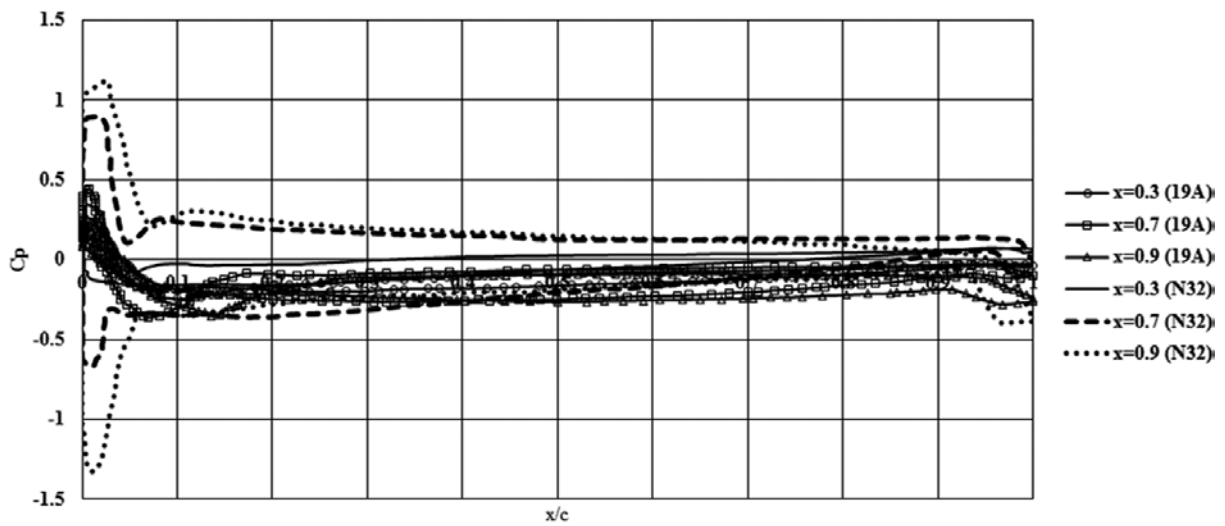


Figure 14. Comparison of the two ducted propeller blade pressure coefficient ($J = 0.8$)

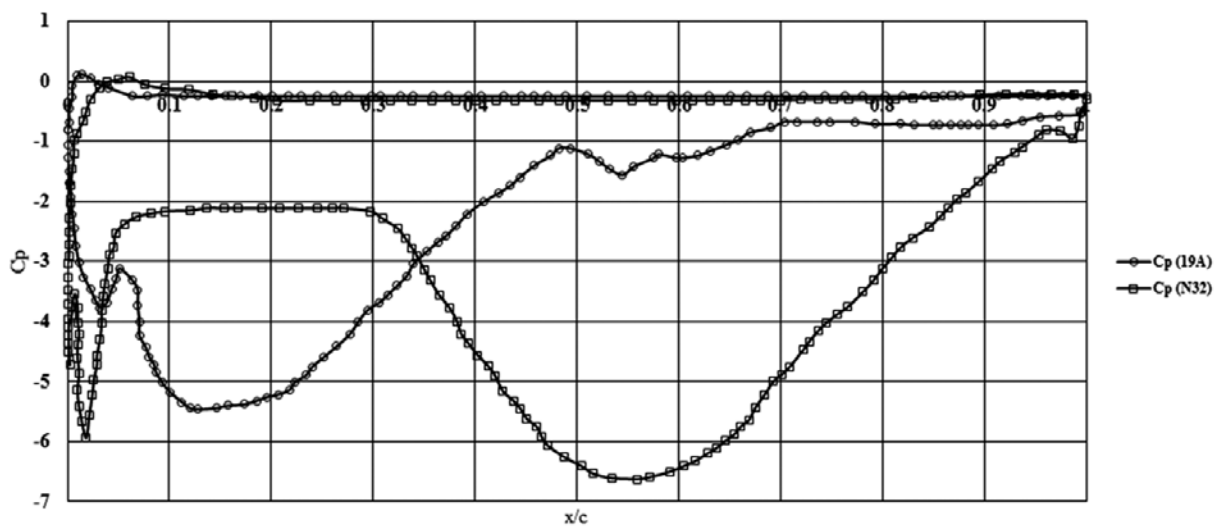


Figure 15. Comparison of the pressure coefficient distribution on ducts ($J = 0.2$)

propellers is illustrated for the back and face of the ducted propellers. In this regard, the side-pressure distribution of both of the ducted propellers' flow field is depicted. The pressure distribution for both back and face sides of the 19A and N32 ducted propeller are illustrated in Figures 16 and 17, respectively. In both ducted propellers, the back pressure is greater than the face one and because of this difference, the propeller thrust is formed.

For the blade tip, because of the pressure jump shown in the blade profile's pressure-coefficient distribution, an instantaneous pressure increase is significant for the propellers.

The flow-field pressure contours containing upstream, the blades back and face and downstream which explains the working and numerical arrangement of the ducted propellers are shown in Figure 18 for both accelerating and decelerating ducts.

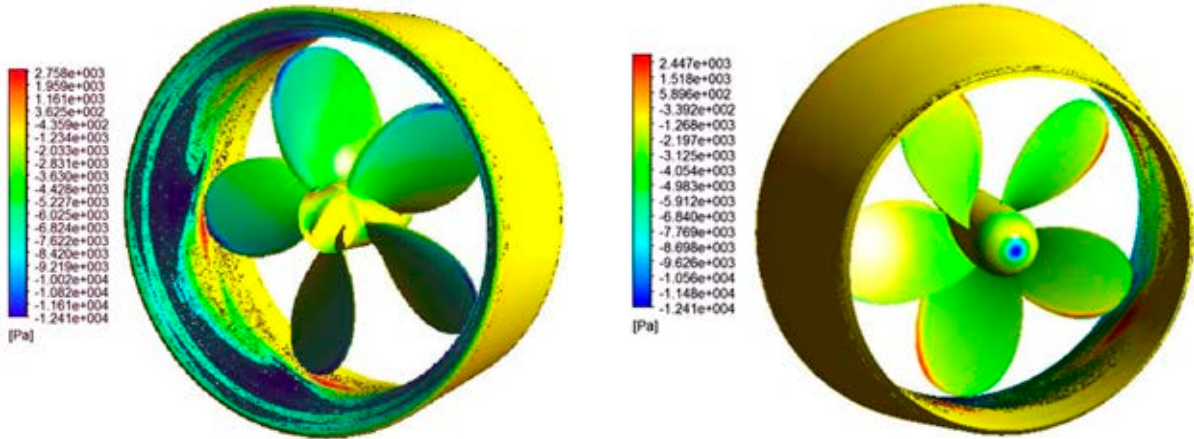


Figure 16. Pressure distribution of the blade surface and the 19A duct ($J = 0.2$)

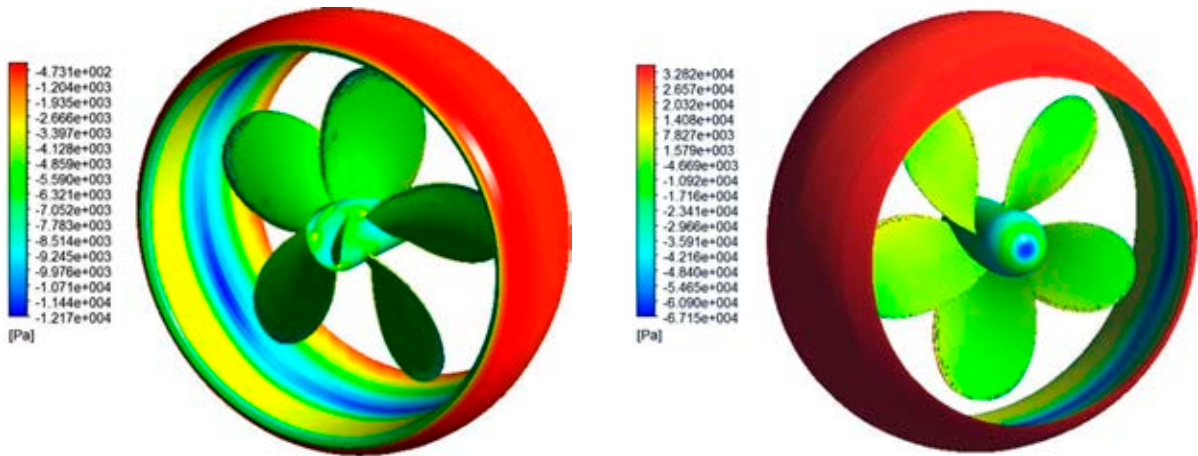


Figure 17. Pressure distribution of the blade surface and the N32 duct ($J = 0.2$)

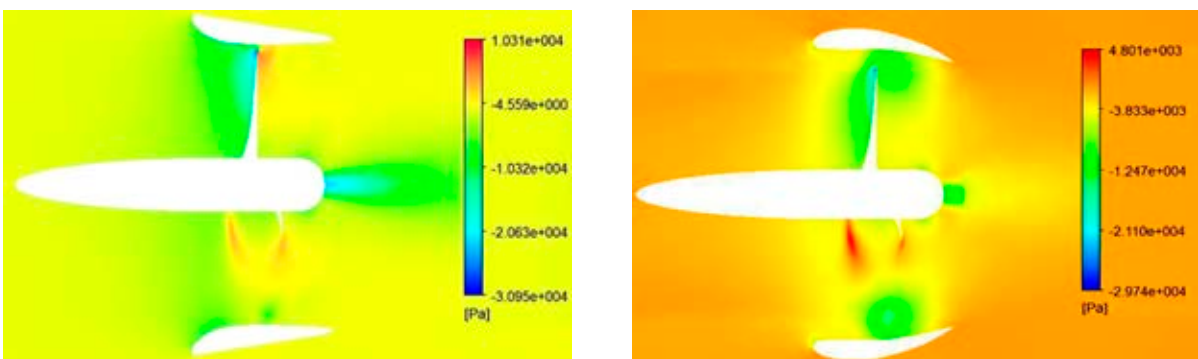


Figure 18. Flow field pressure contour of the 19A and N32 ducted propeller mechanism ($J = 0.2$)

From the pressure contours, it can be seen that the relative pressure at the back of the propeller is more negative than the face so that the back absolute pressure is lower than the face, which results in the thrust in the bossing direction.

Conclusions

In this paper, the effects of the two types of ducts, namely accelerating and decelerating, in combination with a 5-blade propeller have been investigated. The main findings of this research can be summarized as follows:

- From the open-water, hydrodynamic characteristics results, it was observed that the presence of the 19A ducted propeller improved the characteristics of the propeller, while the N32 ducted propeller showed a negative effect on the characteristics. Furthermore, for free, higher-advance ratios, the N32 ducted propeller is suitable and can increase the thrust up to 13 percent, compared with the open-water propeller conditions.
- In moderate conditions ($J = 0.5$), the presence of both ducts had no positive effect on the propulsive thrust. At higher revolutions, in addition, summation of the 19A duct and the blade's thrust was more than the open propeller one. In these conditions, the two ducts thrust was in the same direction as the propeller. In this regards, the total thrust drop of the 19A ducted propeller in $J = 0.8$ was greater than the total thrust drop of the N32 ducted propeller in $J = 0.2$.
- Considering the obtained pressure-coefficient distribution, it was observed that as the distance to the root section increases, both the peak pressure and the leading edge pressure increase. Moreover, it was also found that the pressure coefficient in the suction side of the blade profile was negative.
- Finally, and based on the obtained flow-field pressure contours for the two ducted propellers, it was demonstrated that the lower pressure is always in the back side of the propeller in absence of the ducts. However, based on the contours, adding the ducts has opposite effects on the pressure distribution around the propellers. To be more precise, the accelerating ducts, 19A, will cause more negative pressures in the back side while the N32 type, which is a decelerating one, will result in negative pressure fields in front of the propeller. Therefore, these findings can be applied by engineers for their design purposes.

Acknowledgments

The numerical computations were performed by the HPC of the Marine Engineering Research Center in Amirkabir and Sharif University of Technology. The authors wish to thank the marine group staff for their continuous support.

References

1. ABDEL-MAKSOU, M. & HEINKE, H.-J. (2003) *Scale effects on ducted propellers*. Proceedings of the Twenty-Fourth Symposium on Naval Hydrodynamics, Fukuoka, Japan.
2. ARAZGALDI, R., HAJILOUY, A. & FARHANIEH, B. (2009) Experimental and Numerical Investigation of Marine Propeller Cavitation. *Journal of Scientia Iranica, Sharif University of Technology* 16, 6. pp. 525–533.
3. BALTAZAR, J., RIJPKEMA, D., FALCÃO DE CAMPOS, J. & BOSSCHERS, J. (2013) *A Comparison of Panel Method and RANS Calculations for a Ducted Propeller System in Open-Water*. Third International Symposium on Marine Propulsors (SMP2013), Launceston, Tasmania, Australia, May 2013.
4. BERNITSAS, M.M., RAY, D. & KINELY, P. (1981) *Kt, KQ and Efficiency Curves for Wageningen B-Sereiss Propellers*. Department of Naval and Maritime Engineering, College of Engineering, The University of Michigan.
5. CELIK, F., DOGRUL, A. & ARIKAN, Y. (2011) *Investigation of the Optimum Duct Geometry for a Passenger Ferry*, Yildiz Technical University. IX HSMV Naples 25–27 May 2011, Dept. of Naval Architecture and Marine Engineering, Istanbul, Turkey.
6. GAGGERO, S., RIZZO, C.M., TANI, G. & VIVIANI, M. (2013) *Design, analysis and experimental characterization of a propeller in decelerating duct*. Third International Symposium on Marine Propulsors (SMP2013), Launceston, Tasmania, Australia, May 2013.
7. HE, X., ZHAO, H., CHEN, X., LUO, Z. & MIAO, Y. (2015) Hydrodynamic Performance Analysis of the Ducted Propeller Based on the Combination of Multi-Block Hybrid Mesh and Reynolds Stress Model. *Journal of Flow Control, Measurement & Visualization* 3. pp. 67–74.
8. KOH, K.K., OMAR, Y., AZREEN, E. & NURHASLINA, K. (2015) The Study of Ducted Propeller in Propulsion Performance of a Malaysia Fishing Boat. *Journal Teknologi (Sciences & Engineering)* 74:5 (2015), 39–43, Faculty of Mechanical Engineering, Universiti Teknologi Malaysia.
9. KORT, L. (1934) Der neue Düsenschrauben-Antrieb. *Werft-Reederei-Hafen*, 15. Jahrgang, Heft 4, 41–3.
10. KRASILNIKOV, V.I., SUN, J.Y., ZHANG, Z. & HONG, F. (2007) *Mesh Generation Technique for the Analysis of Ducted Propellers Using a Commercial RANSE Solver and its Application to Scale Effect Study*. Proceedings of the 10th Numerical Towing Tank Symposium (NuTTS'07).
11. MAJDFAR, S. & GHASSEMI, H. (2016) Calculations of the Hydrodynamic Characteristics of a Ducted Propeller Operating in Oblique Flow. *Int. J of Technology*, Preparing Publication.
12. MAJDFAR, S., GHASSEMI, H. & FOROUZAN, H. (2015) Hydrodynamic Effects of the Length and Angle of the Ducted Propeller. *Journal of Ocean, Mechanical and Aerospace – Science and Engineering* 25.

13. MUSZYŃSKI, T. & STRZELCZYK, P. (2013) Experimental Investigation of A Variable Geometry Ducted Propeller. *Advances in Science and Technology Research Journal* 7, 17, March 2013. pp. 56–61.
14. SALVATORE, F., GRECO, L. & CALCAGNI, D. (2011) *Computational analysis of marine propeller performance and cavitation by using an inviscid-flow BEM model*. Second International Symposium on Marine Propulsors, (SMP2011), Hamburg, Germany.
15. SANCHEZ-CAJA, A., RAUTAHEIMO, P. & SIKONEN, T. (2000) *Simulation of incompressible viscous flow around a ducted propeller using a RANS equation solver*. Proceedings of the Twenty-Third Symposium on Naval Hydrodynamics.
16. SPARENBERG, J.A. (1969) On optimum propellers with a duct of finite length. *Journal of Ship Research* 13, 2, pp. 29–136.
17. STIPA, L. (1931) *Experiments with Intubed Propellers*. NACA Technical Report TM 655 (January 1932).
18. SUBHAS, S., SAJI, V.F., RAMAKRISHNA, S. & DAS, H.N. (2012) CFD Analysis of a Propeller Flow and Cavitation. *International Journal of Computer Applications* (0975–8887), 55, 16.
19. VALCIC, M. & DEJHALA, R. (2015) Neural Network Prediction of Open-water Characteristics of Ducted Propeller. *Journal of Maritime & Transportation Sciences* 49–50, 1, April 2015.